CRYSTAL GROWTH & DESIGN
2004
VOL. 4, NO. 2
361−367

Epitaxial Nucleation and Growth of *n*-Alkane Crystals on Graphite (0001)

Mirjam E. Leunissen, W. Sander Graswinckel, Willem J. P. van Enckevort,* and Elias Vlieg

NSRIM Department of Solid State Chemistry, University of Nijmegen, Toernooiveld 1, 6525 ED Nijmegen, The Netherlands

Received May 26, 2003; Revised Manuscript Received November 28, 2003

ABSTRACT: To study the heteroepitaxial growth of apolar organic compounds on apolar inorganic substrates, the *n*-alkanes dotriacontane ($C_{32}H_{66}$) and tritriacontane ($C_{33}H_{68}$), dissolved in *n*-heptane, were deposited onto the (0001) face of highly oriented pyrolytic graphite (HOPG). It was found that both *n*-alkanes display epitaxial crystal growth. The hexagonal symmetry of the substrate surface is reflected by the three preferred orientations of the platelike crystals. The orientation of the alkane crystals was determined using polarization microscopy and atomic force microscopy. A Stranski-Krastanov mechanism for three-dimensional epitaxial growth is proposed, in which the first layer of *n*-alkane molecules on the graphite surface is assumed to be one of the well-known monolayer structures. Three-dimensional nucleation of the *n*-alkane crystals occurs on this layer, in such a way that the hydrocarbon chains of the crystal are parallel to those in the monolayer. From the point group symmetry of the *n*-alkane contact plane and the substrate surface, it was deduced that the epitaxial nuclei of $C_{32}H_{66}$ and $C_{33}H_{68}$ can be deposited in six and three orientations, respectively, which is in agreement with the experimental results.

1 Introduction

During the past decades, many different epitaxial growth systems have been studied, using both organic and inorganic substrates and deposits in all possible combinations. In most studies, the focus is on inorganic−inorganic systems, one of the best known examples being the deposition of one type of semiconductor onto another to produce functional devices. Apart from the early work by Neuhaus,[1] less attention has been given to the deposition of organic substances, both on organic and inorganic substrates. But more recently, after scanning probe microscopy became mature, the interest in these systems has increased (see for instance Salaneck et al.,[2] Koch et al.,[3] and Hooks et al.[4]).

The research currently done is largely restricted to the growth of monolayers. Using layer-by-layer growth to produce thick, single crystalline layers is more difficult because this requires a very close match in lattice parameters of the substrate and the deposited crystals. This is the main bottleneck in producing large single-crystalline layers of organic compounds by this method. An alternative approach involves the growth of numerous three-dimensional nuclei of identical orientation on a suitable substrate, which coalesce to form a single crystal during further growth. In this case, the lattice match is much less critical. This method has proven to be very successful in the growth of single-crystalline gallium nitride layers on sapphire substrates.[5−7]

The three-dimensional nucleation approach makes substrate selection less critical and thus opens possibilities for the growth of crystals that cannot be grown by conventional methods. Also the induced growth of new polymorphs might be achievable, because of stabilizing interactions with the substrate.

Obtaining thick crystal layers by coalescence of oriented three-dimensional nuclei on a suitable substrate requires insight into the heteroepitaxial three-dimensional nucleation processes, the specific conditions which have to be fulfilled for this type of nucleation to occur and the symmetry relationships between the deposit and the substrate. In this paper, we try to expand this insight by investigating the deposition of long-chain *n*-alkanes from *n*-heptane solution onto the (0001) face of highly oriented pyrolytic graphite (HOPG). This acts as a model system for the epitaxial growth of apolar organic compounds on apolar inorganic substrates.

It has now been well established that long chain *n*-alkanes form ordered monolayers on HOPG substrates. Groszek[8] first gave an explanation for the high affinity of *n*-alkanes for HOPG, and Findenegg and coworkers[9,10] were the first to propose the existence of ordered monolayers on the basis of indirect evidence. Soon these layers were directly observed using scanning tunneling microscopy. Two different monolayer structures were found: one in which the *n*-alkane carbon backbone plane is parallel[11] and one in which it is perpendicular to the substrate.[12] In other studies, bilayers were observed as well.[13,14]

However, despite this broad interest in mono- and bilayer adsorption of long chain *n*-alkanes on HOPG, until now few detailed investigations have been carried out of the epitaxial nucleation and growth of three-dimensional crystals and the structural relationship between the substrate, monolayers, and crystallites. To open up this aspect of heteroepitaxy, we report in this paper on the growth of oriented *n*-alkane crystallites on HOPG. We used dotriacontane ($C_{32}H_{66}$) and tritriacontane ($C_{33}H_{68}$) to study possible differences between

* Corresponding author: W. J. P. van Enckevort, NSRIM Department of Solid State Chemistry, Faculty of Science, University of Nijmegen, Toernooiveld 1, 6525 ED Nijmegen, The Netherlands. Phone: +31 (0)24 3653433; fax: +31 (0)24 3653067; e-mail: wvenck@sci.kun.nl.

10.1021/cg0340852 CCC: $27.50
Published on Web 01/16/2004

n-alkanes with odd and even numbers of carbon atoms. Additionally, a few deposition experiments were carried out using tetracosane ($C_{24}H_{50}$) for comparison.

2 Experimental Section

2.1 Crystal Growth. In this study, the *n*-alkane crystals were grown from *n*-heptane solution onto HOPG substrates. As source material, the *n*-alkanes $C_{32}H_{66}$ and $C_{33}H_{68}$, obtained in >99% pure form, were used. The HOPG substrates, which were purchased from Union Carbide, were prepared by cleavage in air using scotch tape. In this way a fresh, crystallographically well-defined (0001) surface was obtained. The substrate was then immersed into a large volume of a dilute solution of one of the *n*-alkanes in *n*-heptane (>99%, Merck, Germany) with a temperature of 45 °C. Both solutions contained 6.08 mmol of *n*-alkane per 100 g of *n*-heptane, i.e., 2.74 g of $C_{32}H_{66}$ and 2.83 g of $C_{33}H_{68}$. After 30−180 s, the sample was removed from the solution and dried gently using a soft tissue. In this way, deposition of disordered *n*-alkane crystals, due to evaporation of excess solution, was prevented.

2.2 Observation Methods. The orientations, shape, and distribution of the deposited *n*-alkane crystallites were examined by means of reflection optical polarization microscopy using a Leitz DMRX polarizing microscope, equipped with a CCD camera. Since the crystallite orientation could not be determined by conventional X-ray powder diffraction methods due to the lateral orientational disorder of the substrate used (it may be possible to acquire this information using nonconventional X-ray methods using a grazing incidence X-ray diffraction setup in combination with synchrotron radiation[15,16]), many individual crystallites were examined with the help of an optical reflection microscope with crossed polarizers. Their crystallographic orientation could be established by determining the extinction directions while viewing the crystallites from the side as well as from the top. Moreover, the polymorph of $C_{32}H_{66}$ was determined using this method.

The morphology of the deposited crystals was studied using a JEOL JSM6340F high-resolution scanning electron microscope. To prevent melting of the crystals due to the high intensity of the electron beam, the SEM was used in cryo mode. After the sample was glued onto the sample holder with a droplet of silver paint, it was quickly frozen in nitrogen slush. In the loading chamber of the microscope any ice crystals formed on the sample were allowed to sublime by leaving the sample for 5 min at −85 °C. Then the sample was cooled to about −140 °C, sputtered with a mixture of gold and palladium, and brought into the microscope chamber. The applied voltage was 1 kV.

The HOPG substrates used were not single crystalline, but were composed of many grains of different orientations, all of them having the hexagonal *c*-axis perpendicular to the top surface. Therefore, the local substrate orientation had to be determined in relation to the *n*-alkane crystallite orientations. This was realized by means of contact mode atomic force microscopy, using a Digital Instruments NanoScope III AFM with silicon nitride cantilevers. First, the crystallites were imaged at low resolution. Then the adjacent HOPG surface was mapped with atomic resolution under ambient conditions, using a scanning speed of 30 lines/s and cantilevers with a nominal spring constant of 0.32 N/m.

3 Observations

3.1 General Features. Characteristic patterns of *n*-alkanes crystallized on (0001) HOPG are shown in Figures 1−3. The deposits of different *n*-alkanes showed no major differences concerning crystal orientations, morphology, and densities. Therefore, in this section we will give general results and will only distinguish between the different *n*-alkanes where relevant.

As verified by in-situ optical reflection microscopy, the epitaxial nucleation of the *n*-alkanes and their subsequent growth occurs during the rapid evaporation of a thin solution film remaining after separation of the sample from the solution. It is essential that the supersaturation at which the crystals are formed is very high and that this value is reached rapidly; otherwise crystals nucleate at impurities or step edges on the substrate. If the liquid layer is too thick or too concentrated for a given evaporation rate the supersaturation increases too slowly and only randomly oriented platelets are formed. During the standard ex-situ experiments, the high supersaturation was obtained by removing most of the solution using a tissue, leaving a very thin layer of solution which then quickly evaporated. Note that such a thin layer can also be obtained by applying a drop of solution on a vertically placed substrate. The solution will flow down the surface leaving a thin layer behind, which will evaporate rapidly. Alternatively, a drop of a very dilute solution can be allowed to evaporate completely on the substrate. Although it is difficult to control the growth conditions exactly, the results are well reproducible.

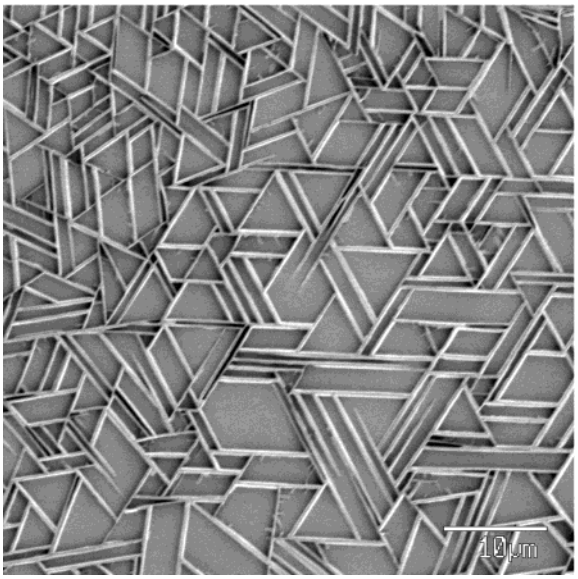

Figure 1. Cryo-SEM image of $C_{32}H_{66}$ on HOPG (0001). At least three domains, each with a different set of three crystallite orientations, can be identified.

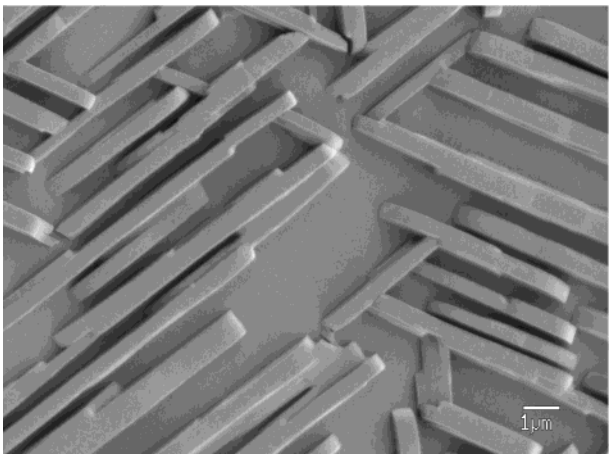

Figure 2. Cryo-SEM image of $C_{33}H_{68}$ on HOPG (0001). The platelet-like crystallites are faceted and are oriented perpendicular to the substrate surface.

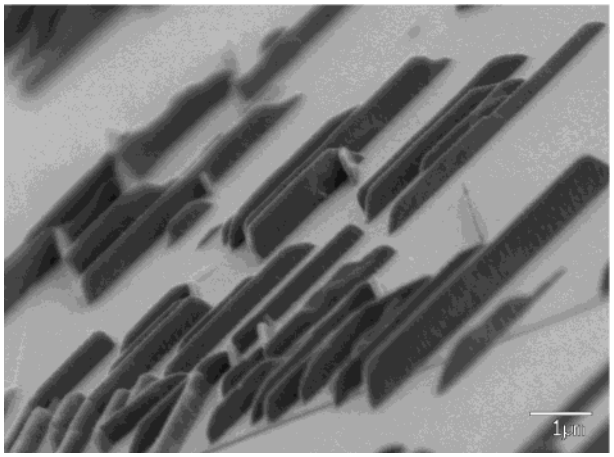

Figure 3. Cryo-SEM image of $C_{32}H_{66}$ on HOPG (0001) viewed from the side. The crystallites all exhibit a platelet-like morphology.

To estimate the supersaturation at which epitaxial crystal growth occurs, a cell was used in which the temperature of both the substrate and the solution could be controlled within 0.1 °C and in which the crystal growth could be observed in-situ.[17] This experiment was only done for $C_{32}H_{66}$. The supersaturation $\Delta\mu$ during the experiments can be calculated using

$$\Delta\mu = kT \ln \frac{c}{c_{eq}} \qquad (1)$$

where c_{eq} is the equilibrium concentration at the substrate temperature and c is the concentration of the bulk solution. At the highest supersaturation that could be reached rapidly in this cell, $\Delta\mu/kT = 0.5$, the growth of small platelike crystals was observed. However, no epitaxial orientation could be seen. The supersaturation required for epitaxial crystal growth is therefore expected to be considerably higher than this value.

In an effort to get an estimate of the actual supersaturation in our growth experiments, the following approach was taken. A drop of a very dilute solution of $C_{32}H_{66}$ in *n*-heptane was deposited on a HOPG substrate and the crystal growth process taking place during rapid evaporation of the solvent was observed in-situ. It was found that at the moment the crystals appeared the solution layer was so thin that interference fringes could be seen. Crystal growth took place close to the last dark fringe visible, from which the layer thickness was estimated to be 1/4 wavelength, which is about 150 nm. This is confirmed by the fact that the average crystal height in these experiments was of the same order. Taking into account the initial layer thickness and concentration and using eq 1 this corresponds to a supersaturation of about $\Delta\mu/kT = 3$.

3.2 Morphology. To interpret the morphologies of the epitaxially grown crystals, "free" *n*-alkane crystals were grown slowly from *n*-heptane solutions. The crystals obtained in this way display the typical morphologies as expected from the literature.[18] Both compounds form thin, lozenge-shaped platelets. $C_{33}H_{68}$ has an orthorhombic crystal structure with space group *Pbcm* ($Z = 4$, $a = 4.96$ Å, $b = 7.48$ Å, and $c = 87.57$ Å). $C_{32}H_{66}$ has both a monoclinic and an orthorhombic polymorph. X-ray powder diffraction of the free crystals showed that

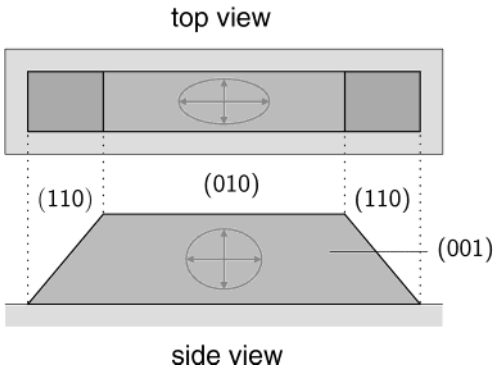

Figure 4. The morphology of epitaxially grown $C_{32}H_{66}$ and $C_{33}H_{68}$ crystallites as determined by polarization microscopy.[22] Both structures are orthorhombic; for $C_{32}H_{66}$ setting $Pbc2_1$ is used. The extinction directions (indicated by arrows) coincide with the crystallographic axes.

the monoclinic structure had been obtained, but in some experiments a small amount of the orthorhombic polymorph was found as well. The monoclinic structure has space group $P2_1/a$ with $Z = 2$, $a = 5.58$ Å, $b = 7.42$ Å, $c = 37.75$ Å, and $\beta = 119°$.[18] For both compounds, the platelets are bounded by large {001} top and bottom faces and four narrow {110} side faces. Sometimes a pair of {010} side faces shows up, which gives the crystals the shape of a hexagon.

If the *n*-alkanes are grown epitaxially on the HOPG surface, both have a similar morphology. As shown in the SEM micrographs of Figures 1−3, like the "free" forms, the crystals are thin platelets. The platelets are oriented perpendicularly, within 2°, to the substrate surface. Two of the narrow side faces are inclined 45−70° with respect to the substrate surface, and the third one is parallel, giving the crystals the appearance of a mirror symmetric trapezium (Figure 3).

From comparing the morphology of a "free" crystal with that of the epitaxially grown crystals, it is clear that the well-developed side faces are the {001} faces. However, we cannot a priori identify the other facets. The faces of the epitaxially grown crystals could not be assigned using conventional X-ray powder diffraction because the signal was too weak compared to the overlapping graphite reflections. Therefore, reflection polarization microscopy was used. When viewing the crystals from the side, i.e., perpendicular to the {001} faces, extinction was found if the polarizers were parallel or perpendicular to the contact plane of the crystallites (see Figure 4). The maximum intensity could be observed at an angle of 45° and 135°. When viewing the crystals from the top, the extinction directions were found to be parallel and perpendicular to the large {001} side faces. For the orthorhombic $C_{33}H_{68}$, this result means that one of the crystallographic axes must be perpendicular to the substrate and another one must be parallel to the substrate. The top face must therefore be either {100} or {010}, the latter being most likely because this face is also part of the morphology of the free paraffin crystals. In addition, a connected net analysis has shown that the {100} faces of the orthorhombic odd *n*-alkanes are easily roughened and thus are not expected to contribute to the growth form.[19] The inclined side faces are therefore most likely {110}. This

assignment is also confirmed by the angles between the faces, although the inclined side faces tend to be quite rounded.

If $C_{32}H_{66}$ crystallizes in the monoclinic polymorph, the extinction directions of the {001} side faces should coincide with the ⟨100⟩ and ⟨010⟩ directions. The fact that the observed extinction occurs for the directions parallel and perpendicular to the substrate implies that the top face is either {100} or {010}. However, AFM as well as SEM have shown that the angle of the top face with respect ot the side faces is exactly 90°, which rules out {100} as the top face. When viewed from the top, the epitaxially grown $C_{32}H_{66}$ shows extinction parallel and perpendicular to the {001} side faces. Additional experiments have shown that, when viewed perpendicularly to the {010} faces, the extinction directions of free monoclinic paraffin crystals are rotated about 30°. Thus, {010} cannot be the top face either. This leads us to conclude that the epitaxially grown crystals are orthorhombic instead of monoclinic with a morphology similar to $C_{33}H_{68}$. Assuming that the structure of orthorhombic $C_{32}H_{66}$ is equivalent to that of orthorhombic $C_{36}H_{74}$,[20] its space group is $Pca2_1$ with $Z = 4$, $a =$ 7.42 Å, $b = 4.96$ Å, and $c = 84.97$ Å. For convenient comparison between both *n*-alkanes, the nonstandard setting $Pbc2_1$ (with $a = 4.96$ Å and $b = 7.42$ Å) will be used in the following.

Special care was taken to ensure that "form birefringence" does not play a role in the polarization microscopy when viewing the crystals from the top. This was done by applying a drop of glycerol to the substrate and gently pressing a microscope cover glass on top of it. The thin glycerol film obtained in this way greatly reduces the difference in refractive index between the crystals and their environment. The results obtained in this way were identical to those mentioned before.

3.3 Distribution. The density of the deposited microcrystals ranged from 10^6-10^7 per mm^2. As a result of the drying process, the distribution of crystals on the surface was not uniform. In many cases, the crystallite sizes were restricted by their nucleation density. After nucleation, a platelet crystal expands in one direction parallel to the substrate until it "collides" with a neighboring one. In this way, a network of crystallites is formed as shown in Figure 1. In a number of other cases, isolated, mostly smaller crystallites were encountered. Both the height and the width of the crystallites were typically between 100 nm and 1 μm.

3.4 Orientation. HOPG has a hexagonal or rhombohedral crystal structure with space group $P6_3/mmc$ and $R\bar{3}m$, respectively. The two-dimensional point group symmetry of the top (0001) surface layer of these crystals is formally $3m$, but in view of the special positions of the carbon atoms in the lattice it is $6mm$. This symmetry is reflected by the preferred orientations of the deposited crystallites, which show angles of 60° with respect to each other. This results in the typical "trigonal" patterns as shown in Figure 1. Since the two-dimensional point groups $3m$ and $6mm$ have 6- and 12-fold multiplicity, respectively, and only three crystallite orientations are observed, this implies that the deposits must be aligned parallel or perpendicularly to one of the mirror lines of the graphite surface. This limits the number of possible crystallite orientations to two, namely, parallel to ⟨100⟩ and parallel to ⟨210⟩ on the graphite surface.

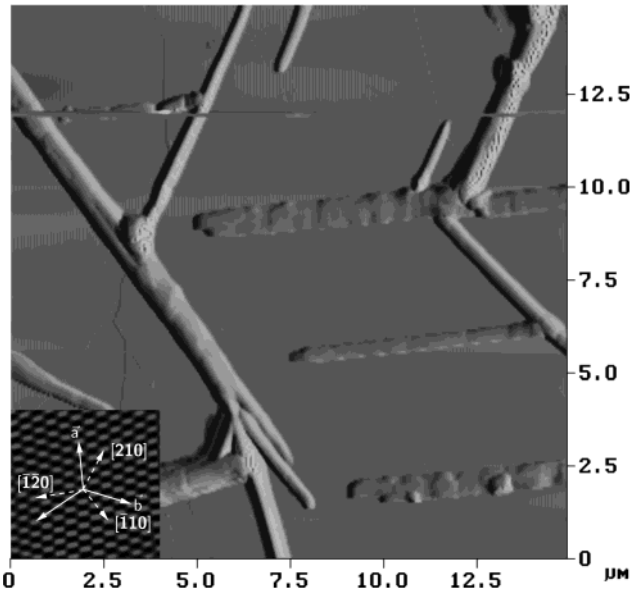

Figure 5. Determination of the $C_{32}H_{66}$ crystallite orientation using AFM. 15 × 15 μm scan showing a number of *n*-alkane crystallites. The inset shows the atomic resolution image of HOPG in the same area after FFT filtering. The directions of the graphite periodic bond chains, which run along the ⟨100⟩ directions are indicated by solid arrows. The set of ⟨210⟩ directions is indicated by dashed arrows. It can be seen that the longitudinal crystallite directions are parallel to the three ⟨210⟩ directions.

The HOPG used is polycrystalline with a grain size of approximately 3 to 50 μm in diameter. All grains are oriented with the hexagonal *c*-axis perpendicular to the substrate surface. The lateral orientations are more or less random. This is the reason for the occurrence of different domains in which all crystals display the same trigonal pattern, but with different orientation in each domain.

The presence of these domains prohibits the application of standard X-ray diffraction techniques to determine the crystallographic orientation (i.e., the direction of the *a*- and *b*-axes) of the substrate with respect to the crystallites. Therefore, we resorted to contact mode AFM (Figure 5). After deposition of *n*-alkane onto the HOPG surface, a large area was imaged to determine the longitudinal direction of the platelike crystals in that area. Then, near one of the imaged crystals, the periodicity of the HOPG surface was imaged in a region of several square nanometers. In the atomic resolution images obtained, every maximum can be thought to represent one six-membered ring of the graphite top layer (see for instance ref 21). From this information, the directions of the periodic bond chains (PBCs), i.e., the zigzag chains of bonded carbon atoms along the ⟨100⟩ directions in the graphite structure, could be determined.

Comparison of these orientations with crystallite directions in the same domain showed that the $C_{32}H_{66}$ and $C_{33}H_{68}$ platelets are always oriented with their longitudinal direction perpendicular to the ⟨100⟩ carbon chains of the graphite lattice.

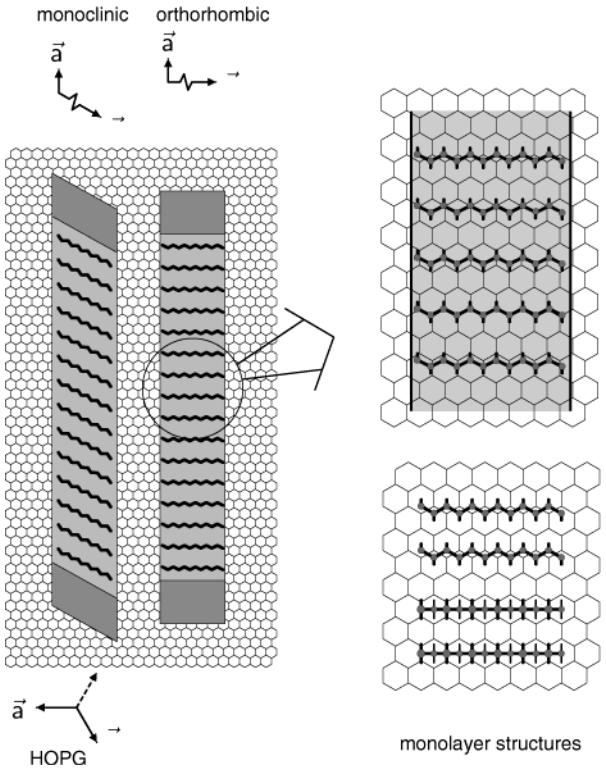

Figure 6. Morphology, orientation, and contact face of the epitaxial *n*-alkane crystals on HOPG (0001). The longitudinal direction of the platelet-like crystallites is parallel to the ⟨210⟩ directions of the substrate. The contact face is {010}. The direction of the *n*-alkane chains in the crystals is indicated. In the orthorhombic crystal structure, the chains are perpendicular to the opposite (001) and (00$\bar{1}$) faces. In the monoclinic crystal, which was not found to grow epitaxially on graphite, the carbon chains are inclined. In addition to the crystallites, the two possible monolayer structures are depicted. In both structures, the chains are parallel to ⟨100⟩; in the first structure the backbone plane of the molecules is parallel to the substrate, and in the second structure it is perpendicular to the substrate.

The morphology, crystallographic orientation, and contact face of the crystals with respect to the substrate lattice are summarized in Figure 6.

4 Discussion

4.1 Epitaxial Growth Mechanism. Many cases of *n*-alkane monolayer formation on HOPG substrates have been reported in the literature.[11,12,23] These scanning tunneling microscopy studies show that ordered layers develop for a wide range of temperatures and concentrations of the applied solution. Even if very dilute solutions are used, monolayers still develop. In our experiments, the presence of a monolayer could not be revealed by AFM. This is not unexpected in view of the difficulty of imaging physisorbed molecules using a standard version of this technique.[24] From the above, it follows that, very probably, at the beginning of heteroepitaxial *n*-alkane nucleation a monolayer already has been formed. The directions of the *n*-alkane chains in the monolayer structures reported in the literature are parallel to the zigzag C−C chains, i.e., the ⟨100⟩ directions, of the graphite substrate. The carbon backbone plane of the *n*-alkane chains can be perpendicular as well as parallel to the graphite (0001) plane.[11,12]

In general, *n*-alkane crystals have a lamellar structure, which consists of a stacking of layers of parallel *n*-alkane chains.[18] In the orthorhombic polymorph the *n*-alkane chains are perpendicular to the {001} planes. It was shown in the previous section that the longitudinal direction of the platelet-like deposits is perpendicular to the carbon chains of the substrate. For the orthorhombic *n*-alkane crystals the molecules, which are parallel to the *c*-axis, are oriented parallel to the graphite carbon chains (Figure 6). Therefore they have the same orientation as the molecules in the monolayer structure. The backbone plane of the molecules in the crystallites is inclined about 45° with respect to the (0001) graphite surface.

The distance between two paraffin molecules in the monolayer structure on HOPG is 4.2 Å.[23] The distance between two molecules on the {010} surface of orthorhombic $C_{32}H_{68}$ and $C_{33}H_{68}$ is 5.0 Å. Thus, there is a relatively large lattice mismatch between the crystal and the monolayer on which the crystals are assumed to nucleate. Concluding, we propose the growth mechanism of epitaxial *n*-alkane crystals on graphite to be Stranski-Krastanov type:[25,26] first, a monolayer is formed, and then three-dimensional epitaxial nucleation takes place on the monolayer.

Because the orientation of the molecules in the monolayer is the same as in the orthorhombic crystals, whereas this is not the case for the monoclinic polymorph, it seems likely that the monolayer acts as a template on which the orthorhombic polymorph of $C_{32}H_{66}$ is formed preferentially. However, the rather harsh growth conditions could also play a role. To investigate the influence of the growth conditions, crystals were grown under the same conditions but on a substrate other than graphite. X-ray diffraction showed that a mixture of orthorhombic and monoclinic crystals had been obtained. This means that the occurrence of the orthorhombic modification is at least partly caused by the growth conditions. However, the epitaxially grown crystals on graphite are orthorhombic exclusively, so this process indeed shows promise for the nucleation of specific polymorphs.

4.2 Triclinic $C_{24}H_{50}$. For comparison, tetracosane ($C_{24}H_{50}$), a member of the family of paraffins that crystallize in the triclinic system, was grown epitaxially on HOPG as well. It was found to show the same pattern as $C_{32}H_{66}$ and $C_{33}H_{68}$ (Figure 7). Despite partial melting due to the low melting point of this compound the orientation of the crystallites could also be determined using AFM. Interestingly, the orientation turned out to be the same as that of the other paraffins studied; that is, the longitudinal axis of the crystals is perpendicular to the ⟨100⟩ PBCs of the substrate. Unfortunately, attempts to determine the contact face of the crystals were unsuccessful.

4.3 Critical Nucleus Size. An estimate of the size of a critical embryo gives an idea of what length scale the process of 3D heteroepitaxial nucleation of the *n*-alkanes on graphite takes place. It must be stressed that in the following we assume that the critical nucleus is spherical. Due to the highly anisotropic morphology of paraffin crystals, the nucleus is probably nonspherical. A more detailed analysis is beyond the scope of this paper, however.

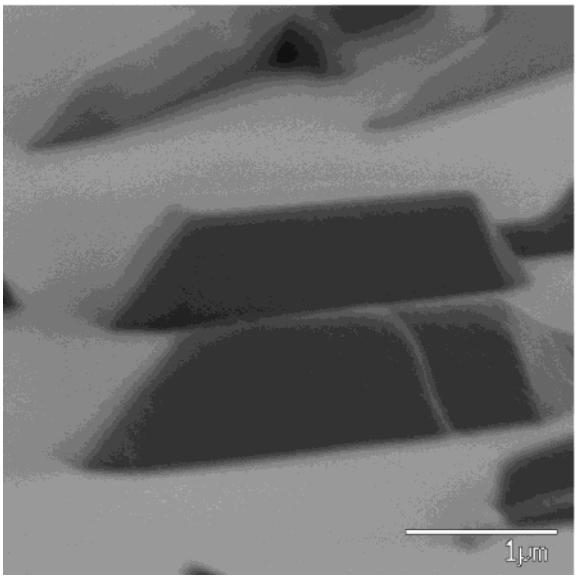

Figure 7. Cryo-SEM image of $C_{24}H_{50}$ on HOPG (0001) viewed from the side.

From classical nucleation theory, it is known that the radius of a (spherical) critical nucleus equals:[27−29]

$$r^* = \frac{2\gamma\Omega}{\Delta\mu} \tag{2}$$

In this equation, Ω is the volume of one growth unit, γ is the surface free energy of the crystallite in contact with the solution, and $\Delta\mu$ is the difference in thermodynamic potential of the solute and the solid. For orthorhombic $C_{32}H_{66}$ the volume of one growth unit is 782 Å^3.[18]

As mentioned in section 3.1, epitaxial crystal growth takes place at an estimated supersaturation of $\Delta\mu/kT = 3$ for $C_{32}H_{66}$. If one assumes that the equivalent wetting condition[30] is fulfilled, the surface energy γ can be roughly estimated from the heat of dissolution ΔH_{diss} per molecule according to

$$\gamma \approx \frac{\Delta H_{\mathrm{diss}}}{A} \tag{3}$$

In this equation, A is the surface area of one rod-shaped molecule, which is calculated from the X-ray structure to be 560 Å^2. Equivalent wetting implies that the interactions of solvent molecules with molecules at the crystal surface and with solute molecules are identical. The heat of dissolution is derived from the solubility of $C_{32}H_{66}$ in *n*-heptane as a function of temperature, using

$$\ln c_{\mathrm{eq}} = \frac{\Delta H_{\mathrm{diss}}}{kT} - \frac{\Delta S}{k} \tag{4}$$

where ΔS is the entropy of dissolution. From solubility data reported in the literature[31,32] and obtained at our laboratory, ΔH_{diss} was determined to be 1.6×10^{-19} J/molecule. This gives $\gamma = 29$ mJ/m^2. This value is not far from that measured for $C_{23}H_{48}$ in hexane (20.6 mJ/m^2,[33]) and $C_{28}H_{58}$ grown from petroleum ether (28.7 mJ/m^2,[34]).

From the experiments described in section 3.1 and using eq 2, we now obtain an estimated value for the radius of the critical nucleus of $r^* = 36$ Å for $C_{32}H_{66}$ at a substrate temperature of 30 °C. This corresponds to about 250 molecules. However, the number of paraffin molecules in the critical heteroepitaxial nucleus on the graphite substrate also depends on the crystal−substrate interfacial energy of the contact face. From the theory of anisotropic nucleation, it follows that a critical nucleus on a foreign substrate can be considered as a critical free nucleus that is cut along a plane parallel to the contact face.[27] Now, comparing the shapes of the epitaxial crystallites with the "free" crystals,[35] they appear to be cut just below the (010) face, reducing their volume by at least 1 order of magnitude. This reduces the size of the critical nucleus, and thus the number of molecules in it, by the same amount.

Multiplicity of Orientation. In the case of epitaxial growth, the number of symmetrically equivalent orientations of the deposited crystals is determined by the two-dimensional point groups of the substrate surface and the contacting face of the guest crystals. The set of symmetry operators of the two-dimensional point group of the substrate surface is given by $\mathbf{S_{sub}} = \{S_{s,1} = E, S_{s,2}, S_{s,3}, \cdots, S_{s,m}\}$. For the contact face of the deposited crystal, the two-dimensional point group is defined by $\mathbf{S_{crys}} = \{S_{c,1} = E, S_{c,2}, S_{c,3}, \cdots, S_{c,m'}\}$. E is the unit operator. Starting from these sets, it can be shown that the number of possible overlayer domains with a different orientation is given by

$$n = \frac{N(\mathbf{S_{sub}})}{N(\mathbf{S_{sub}} \cap \mathbf{S_{crys}})} \tag{5}$$

In this equation $N(\mathbf{S})$ is the number of elements of the set $\mathbf{S}$, whereas $\mathbf{S_{sub}} \cap \mathbf{S_{crys}}$ is the intersection of the two sets involved.

This formula can be applied to the growth of $C_{32}H_{66}$ and $C_{33}H_{68}$ crystals on the HOPG (0001) surface. The 2D point group of the graphite substrate surface is $6mm$, which has a multiplicity of $N(\mathbf{S_{sub}}) = 12$. The space group of the orthorhombic $C_{33}H_{68}$ is $Pbcm$, and therefore its point group is mmm. From this it follows that the two-dimensional point group of the (010) contact face is $2mm$, so $N(\mathbf{S_{crys}}) = 4$. Since the paraffin *c*- and *a*-axes are aligned with two perpendicular mirror planes in $6mm$, $N(\mathbf{S_{sub}} \cap \mathbf{S_{crys}}) = 4$. So the number of different crystallite orientations will be 3 for $C_{33}H_{68}$ on graphite (0001), which agrees with the experimental observations.

The space group of orthorhombic $C_{32}H_{66}$ is $Pca2_1$, and its associated point group is therefore $mm2$. The two-dimensional point group of the (010) contact face is m, which gives $N(\mathbf{S_{crys}}) = 2$. From this it follows that $N(\mathbf{S_{sub}} \cap \mathbf{S_{crys}}) = 2$, which means that six possible orientations exist for $C_{32}H_{66}$ on (0001) graphite. Taking into account the fact that a rotation of 180° around [010] cannot be distinguished using the experimental techniques available, this result is, again, in agreement with the observations.

Conclusions

In this paper, we have examined the phenomenon of three-dimensional heteroepitaxial growth of apolar long chain *n*-alkane crystals on apolar HOPG (0001) substrates from solution. The grown crystallites were

examined using optical (polarization) microscopy, SEM, AFM, and X-ray diffraction. The platelet shaped paraffin crystals have strongly preferred orientations, the "trigonal" pattern of which reflects the hexagonal symmetry of the substrate surface. For $C_{32}H_{66}$ and $C_{33}H_{68}$, we determined the contact plane to be (010) with the in-plane axis ⟨100⟩ parallel to the ⟨210⟩ directions of the substrate surface. This means that the orientation of the molecules in the crystal is the same as that of the *n*-alkane molecules in the monolayer on the graphite substrate. There is, however, no exact lattice match between the contact face of the crystal and the monolayer. Therefore, we propose a Stranski-Krastanov type growth mechanism. First, a monolayer is formed, and then three-dimensional nucleation of *n*-alkane crystals takes place on this layer. All epitaxially oriented crystals of $C_{32}H_{66}$ were found to have the thermodynamically less stable orthorhombic structure. This selective nucleation of the orthorhombic polymorph is probably caused by a combination of the growth process and the presence of the graphite substrate.

References

(1) Neuhaus, A. *Fortschr. Mineral.* **1950**, *1*, 136−296.
(2) Salaneck, W. R. *Crit. Rev. Solid State Mater. Sci.* **1985**, *12*, 267−296.
(3) Koch, E. E. *Phys. Scr.* **1987**, *T17*, 120−136.
(4) Hooks, D. E.; Fritz, T.; Ward, M. D. *Adv. Mater.* **2001**, *13*, 227−241.
(5) Amano, H.; Sawaki, N.; Akasaki, I.; Toyoda, Y. *Appl. Phys. Lett.* **1986**, *48*, 353−355.
(6) Akasaki, I.; Amano, H.; Koide, Y.; Hiramatsu, K.; Sawaki, N. *J. Cryst. Growth* **1989**, *98*, 209−219.
(7) de Theije, F. K.; Zauner, A. R. A.; Hageman, P. R.; van Enckevort, W. J. P.; Larsen, P. K. *J. Cryst. Growth* **1999**, *197*, 37−47.
(8) Groszek, A. J. *Proc. R. Soc. London Ser. A* **1970**, *314*, 473−498.
(9) Kern, H. E.; Piechocki, A.; Brauer, U.; Findenegg, G. H. *Prog. Colloid Polym. Sci.* **1978**, *65*, 118−124.
(10) Findenegg, G. H.; Liphard, M. *Carbon* **1987**, *25*, 5, 119−128.
(11) McGonigal, G. C.; Bernhardt, R. H.; Thomson, D. J. *Appl. Phys. Lett.* **1990**, *57*, 28−30.
(12) Rabe, J. P.; Buchholz, S. *Science* **1991**, *253*, 424−427.
(13) Watel, G.; Thibaudau, F.; Cousty, J. *Surf. Sci. Lett.* **1993**, *281*, L297−L302.
(14) Gilbert, E. P.; White, J. W.; Senden, T. J. *Chem. Phys. Lett.* **1994**, *227*, 443−446.
(15) Weinbach, S. P.; Weissbuch, I.; Kjaer, K.; Bouwman, W. G.; Als-Nielsen, J.; Lahav, M.; Leiserowitz, L. *Adv. Mater.* **1995**, *7*, 862−863.
(16) Kuzmenko, I.; Rapaport, H.; Kjaer, K.; Als-Nielsen, J.; Weissbuch, I.; Lahav, M.; Leiserowitz, L. *Chem. Rev.* **2001**, *101*, 1659−1696.
(17) Graswinckel, W. S., et al., 2002, work in progress.
(18) Boistelle, R. In *Current Topics in Materials Science*; Kaldis, E., Ed.; North-Holland Publishing Company: Amsterdam, 1980; Vol. 4, Chapter 8, pp 413−479.
(19) Bennema, P.; Liu, X. Y.; Lewtas, K.; Tack, R. D.; Rijpkema, J. J. M.; Roberts, K. J. *J. Cryst. Growth* **1992**, *121*, 679−696.
(20) Teare, P. *Acta Crystallogr.* **1959**, *12*, 294−300.
(21) Hölscher, H.; Schwarz, U.; Zwörner, O.; Wiesendanger, R. *Phys. Rev. B* **1998**, *57*, 2477−2481.
(22) Wahlstrom, E. E. *Optical Crystallography*; John Wiley and Sons: New York, 1979.
(23) Couto, M.; Liu, X. Y.; Bennema, P. *J. Appl. Phys.* **1994**, *75*, 627−629.
(24) Gotsmann, B.; Schmidt, C.; Seidel, C.; Fuchs, H. *Eur. Phys. J. B* **1998**, *4*, 267−268.
(25) Venables, J. A.; Spiller, G. D. T.; Hanbücken, M. *Rep. Prog. Phys.* **1984**, *47*, 399−459.
(26) Greene, J. E. In *Handbook of Crystal Growth*; Thermodynamics and Kinetics: Nucleation Theory; Hurle, D. T. J., Ed.; Elsevier: Amsterdam, 1993; Vol. 1, Part A, Chapter 9.
(27) Mutaftschiev, B. In *Fundamentals, Thermodynamics and Kinetics*, Vol. 1a of *Handbook of Crystal Growth*; Hurdle, D. T. J., Ed., Elsevier: Amsterdam, 1993; Chapter 4, pp 187−248.
(28) Liu, X. Y. In *Advances in Crystal Growth Research*; Sato, K., Furukawa, Y., Nakajima, K., Eds.; Elsevier: Amsterdam, 2001; Chapter 3.
(29) Kashchiev, D. *Nucleation, Basic Theory with Applications*; Butterworth-Heinemann: Oxford, 2000.
(30) Bennema, P. In *Handbook of Crystal Growth*; Thermodynamics and Kinetics: Nucleation Theory; Hurle, D. T. J., Ed.; Elsevier: Amsterdam, 1993; Vol. 1, Part A, Chapter 7.
(31) Roberts, K. L.; Rousseau, R. W.; Teja, A. S. *J. Chem. Eng. Data* **1994**, *39* (4), 793−795.
(32) Madsen, H. E. L.; Boistelle, R. *J. Chem. Soc., Faraday Trans. 1* **1976**, *72*, 1078−1081.
(33) van Hoof, P. J. C. M.; van Enckevort, W. J. P.; Schoutsen, M. *J. Cryst. Growth* **1998**, *193*, 679−691.
(34) Boistelle, R.; Doussoulin, A. *J. Cryst. Growth* **1976**, *33*, 335−352.
(35) van Hoof, P. J. C. M.; Grimbergen, R.; Meekes, H.; van Enckevort, W.; Bennema, P. *J. Cryst. Growth* **1998**, *191*, 861−872.

CG0340852